Estimation of Elongational Viscosity of Polymers from Entrance Loss Data Using Individual Parameter Optimization

MAHESH GUPTA

Mechanical Engineering–Engineering Mechanics Department, Michigan Technological University, Houghton, Michigan 49931

Received: February 22, 2001
Accepted: January 28, 2002

ABSTRACT: The elongational viscosity model proposed by Sarkar and Gupta (Journal of Reinforced Plastics and Composites 2001, 20, 1473), along with the Carreau model for shear viscosity is used for a finite element simulation of the flow in a capillary rheometer. The entrance pressure loss predicted by the finite element flow simulation is matched with the corresponding experimental data to predict the parameters in the elongational viscosity model. To improve the computational efficiency, various elongational viscosity parameters are optimized individually. Estimated elongational viscosity for a Low Density Polyethylene (Dow 132i) is reported for two different temperatures. © 2002 Wiley Periodicals, Inc. Adv Polym Techn 21: 98–107, 2002; Published online in Wiley Interscience (www.interscience.wiley.com). DOI 10.1002/adv.10017

Introduction

The generalized Newtonian constitutive models[1] with shear-thinning viscosity have been commonly employed to simulate polymeric flows. Even though the generalized Newtonian models can accurately simulate the shear-dominated flows such as those encountered in plastic molding processes, the simulation of an elongation-dominated flow, such as the flow in extrusion dies, with this simplified approach can have a large error. The primary reason for the poor prediction of an

Correspondence to: Mahesh Gupta; e-mail: mahesh@mtu.edu.

Advances in Polymer Technology, Vol. 21, No. 2, 98–107 (2002)

elongation-dominated flow is the low elongational viscosity of the generalized Newtonian models.[1] The long chain polymer molecules exhibit stiff resistance to an elongational deformation. Therefore, the elongational viscosity of a polymer, which is defined as the ratio of the elongational stress to elongational strain rate, is very high. An accurate knowledge of the elongational viscosity of a polymer is important for simulating the elongation-dominated flows.

Various techniques such as uniaxial extension, lubricated compression, fiber spinning, bubble collapse, stagnation flow, etc., have been used in the past to experimentally characterize the elongational viscosity of polymers. A good review of these techniques and the difficulties associated with each of these techniques is presented by Macosko.[2] Among these, the most commonly used technique is the uniaxial extension. An elongational rheometer using uniaxial extension, which is based upon Meissner's work,[3] is currently marketed by Rheometric Scientific, Inc., Piscataway, New Jersey, (http://www.rheosci.com). However, maintaining a steady uniaxial extensional deformation is difficult at a high elongation rate.[2] Therefore, Meissner's technique can be used to determine elongational viscosity only at very low elongation rates ($<10\ s^{-1}$). Also, Meissner's technique can only be used for highly viscous melts. Since the deformation rate in polymer processing can range from 1000 to 100,000 s^{-1}, this technique cannot provide the elongational viscosity data required for simulation of most polymer processing techniques.

Because of the difficulties associated with direct measurement of elongational viscosity of a polymer, the flow in a channel with abrupt contraction (entrance flow) has often been used for an indirect measurement of elongational viscosity.[2] A fluid going through an abrupt contraction experiences a rapid elongational deformation. Therefore, if the fluid has a high elongational viscosity, to maintain the elongational flow, a large pressure gradient is required near the contraction. Accordingly, for a polymer going through an abrupt contraction, a steep pressure drop, called entrance pressure loss is encountered near the abrupt contraction. The value of entrance pressure loss, which depends upon the flow rate in the channel, can be used for an indirect measurement of the strain-rate dependence of the elongational viscosity of a polymer. The advantage of the entrance flow method for measuring elongational viscosity is its applicability at high elongation rates. Furthermore, an existing capillary rheometer, which is commonly used for measuring shear viscosity, can also be used for elongational viscosity estimation.

Assuming that the pressure loss in an entrance flow can be obtained by summing the pressure drops due to shear and elongational deformations, Cogswell[4] obtained separate expressions for these two pressure drops. To further simplify the analysis, Cogswell made several other assumptions listed below:

1. Shear stress (τ) and shear rate ($\dot{\gamma}$) are related by power-law model ($\tau = A\dot{\gamma}^n$);
2. Elongational viscosity is constant;
3. The interface between the recirculation region and the main flow is a conical surface (funnel-shaped flow);
4. No-slip on the interface between recirculation region and the main flow;
5. Fully developed flow with zero radial velocity;
6. Neglect Weissenberg–Robinowitsch correction[1];
7. Isothermal, inertia-less, incompressible flow with no normal stresses in shear.

With these assumptions, Cogswell performed a force balance on a differential section of the funnel-shaped entry region near abrupt contraction. By integrating the expressions thus obtained, Cogswell obtained the following expressions for average elongation rate ($\dot{\varepsilon}_a$) in entrance flow and the corresponding elongational viscosity (η_e) for an axisymmetric flow.

$$\dot{\varepsilon}_a = \frac{4\tau_w \dot{\gamma}_a}{3(n+1)\Delta p_e} \tag{1}$$

$$\eta_e = \frac{3(n+1)\Delta p_e}{8\dot{\varepsilon}_a} \tag{2}$$

where $\tau_w = \Delta p R/2L$ is the shear stress at the capillary wall, $\dot{\gamma}_a = 4Q/(\pi R^3)$, Δp, and Q are respectively, the pressure drop and flow rate in the capillary, R and L are the radius and length of the capillary, respectively, and Δp_e is the entrance pressure loss.

By removing some of the assumptions in the Cogswell's analysis, Binding[5] obtained a more accurate expression for entrance pressure loss in an abrupt contraction. However, many of the assumptions in Cogswell's analysis, listed below, are retained in Binding's analysis:

1. Power-law model for shear viscosity ($\eta_s = A\dot{\gamma}^{n-1}$) as well as for elongational viscosity ($\eta_e = B\dot{\varepsilon}^{m-1}$);
2. The interface between the recirculation region and the main flow is a conical surface (funnel-shaped flow);
3. No-slip on the interface between recirculation region and the main flow;
4. Fully developed flow with no radial velocity;
5. $|\mathrm{d}R/\mathrm{d}z| \ll 1$, such that the terms involving $(\mathrm{d}R/\mathrm{d}z)^2$ and $\mathrm{d}^2R/\mathrm{d}z^2$ can be neglected, implying a large recirculation zone;
6. Energy consumed in recirculation zone can be neglected;
7. Isothermal, inertia-loss, incompressible flow with no normal stresses in shear.

With these simplifications, Binding employed energy principles to obtain the following equation for entrance pressure loss:

$$\Delta p_e = \frac{2A(1+m)^2}{3m^2(1+n)^2}\left[\frac{mB(3n+1)n^m I_{nm}}{A}\right]^{\frac{1}{m+1}} \times \dot{\gamma}_w^{\frac{m(n+1)}{m+1}}\left[1-\alpha^{\frac{3m(n+1)}{m+1}}\right] \quad (3)$$

where $\alpha = R_0/R_1$, with R_0 and R_1 being the radii of downstream and upstream channels respectively, $I_{mn} = \int_0^1 |((3n+1)\rho^{1+1/n}/n) - 2|^{m+1}\rho\,\mathrm{d}\rho$, and the shear rate at capillary wall $\dot{\gamma}_w = (3n+1)Q/(\pi n R_0^3)$. If the power-law model for shear viscosity of a polymer, and entrance pressure loss is known for two different flow rates in an abrupt contraction, Eq. (3) can be used to determine the power-law model for the elongational viscosity (B, m) of the polymer.

By using independent power-law models for shear and elongational viscosities, Gupta[6] analyzed the effect of elongational viscosity on vortex formation and entrance pressure loss in an axisymmetric 4:1 entrance flow. Similar analyses of the flow in a channel with abrupt contraction for the planar[7] and the three-dimensional[8] cases have also been presented. The truncated power-law model was used for the shear viscosity as well as for the elongational viscosity in the axisymmetric and planar cases.[6–8] This approach for simulating polymeric flows is frame invariant. Also, if irrespective of the value of e_{II}, the specified shear and elongational viscosity models are such that $\eta_e(e_{II}) = \beta\eta_s(e_{II})$, with $\beta = 3$ for axisymmetric flows, $\beta = 4$ for planar flow, and e_{II} being the second invariant of the strain-rate tensor, then for any three-dimensional flow, the velocity and pressure distributions predicted by this approach are identical to those from the generalized Newtonian formulation. It should be noted that $\eta_e(e_{II}) = \beta\eta_s(e_{II})$ is satisfied by all generalized Newtonian models. More recently, using the same approach, Sarkar and Gupta[9] employed the Carreau model for shear viscosity

$$\eta_s = \eta_0(1+(\lambda e_{II})^2)^{\frac{n-1}{2}} \quad (4)$$

and the following modification of the Carreau model for elongational viscosity

$$\eta_e = \eta_0\left[3+\delta\left\{1-\frac{1}{\sqrt{1+(\lambda_1 e_{II})^2}}\right\}\right][1+(\lambda_2 e_{II})^2]^{\frac{m-1}{2}} \quad (5)$$

For $\delta = 0$, the elongational viscosity model in Eq. (5), reduces to the Carreau model with the elongational viscosity parameters λ_2 and m, respectively, replacing λ and n in the shear viscosity model. It is evident from Fig. 1 that the parameter λ_1 in Eq. (5) specifies $1/e_{II}$ for transition between Newtonian and elongation-thickening portions of the viscosity strain–rate curve, whereas δ characterizes the total increase in viscosity in the elongation-thickening portion. Parameters λ_2 and m in Eq. (5) specify $1/e_{II}$ for transition between elongation-thickening and power-law regions, and the power-law index for elongational viscosity, respectively.

In this work, we have used the Carreau model for shear viscosity [Eq. (4)] and the model proposed by Sarkar and Gupta for elongational viscosity [Eq. (5)]. Knowing the shear and elongational viscosity parameters, a finite element simulation of the entrance flow is performed. The finite element simulation of the entrance flow eliminates most of the simplifying assumptions of Cogswell's and Binding's analyses. However, the flow simulation still assumes an isothermal, inertia-less, incompressible flow with no normal stresses in a shear flow. With a knowledge of the shear viscosity and entrance pressure loss, using the procedure presented in the next section, the elongational viscosity parameter are optimized such that the difference between the experimental values of entrance pressure loss and the corresponding predictions from the finite element simulation is minimized.

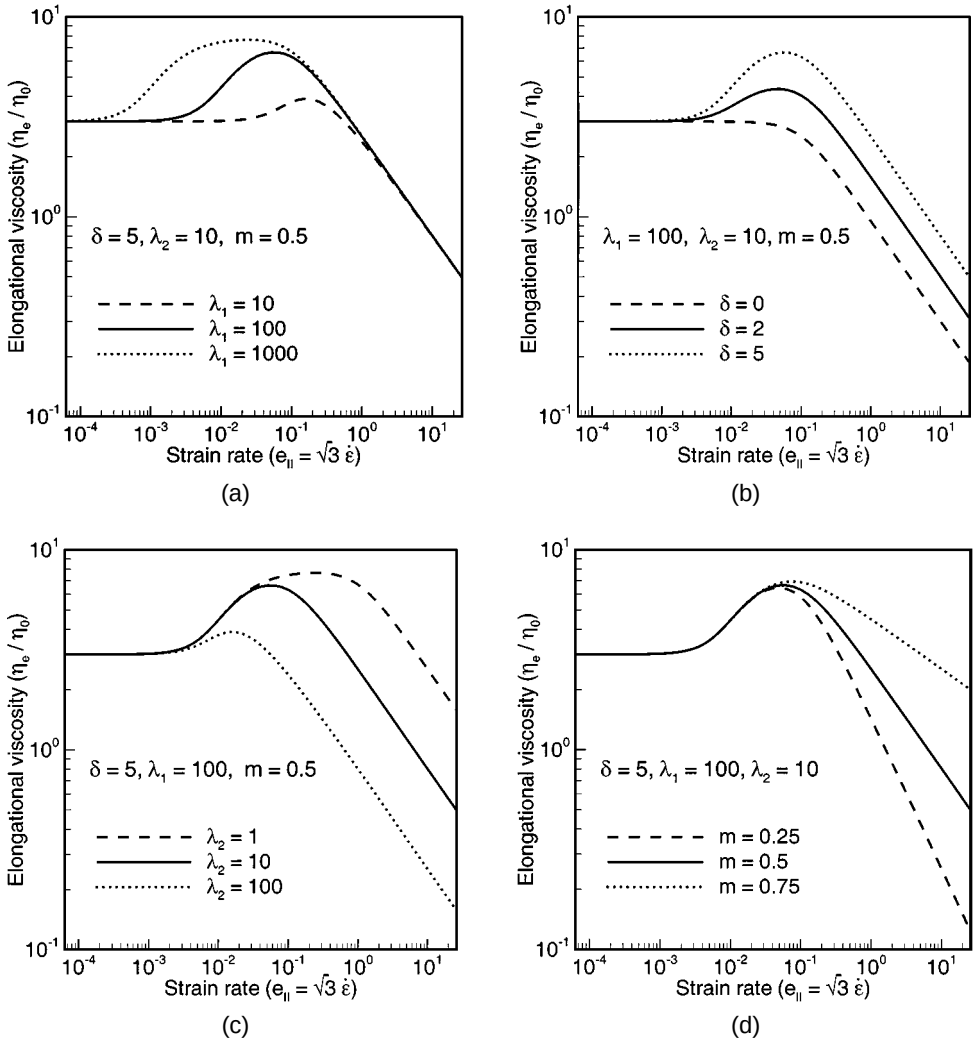

FIGURE 1. Effect of various parameters in Eq. (5), λ_1 (a), δ (b), λ_2 (c), and m (d), on elongational viscosity.

Estimation Procedure for Elongational Viscosity Parameters

Earlier we reported a minimization procedure for simultaneous optimization of all four elongational viscosity parameters (δ, λ_1, λ_2, and m).[10] In particular, starting with an initial guess for the four parameters, the simplex optimization scheme was used to iteratively improve their values such that the difference between experimental and predicted values of entrance loss is minimized. Even though such a global minimization procedure is more rigorous, and attempts to minimize the error over the complete range of flow rate vs entrance loss data, it requires very large amount of computational time, and convergence to the optimal values is prohibitively slow at times. It should be noted that the main reason for the slow convergence is not the simplex optimization scheme, but the simultaneous optimization of the all four elongational viscosity parameters, which requires repeated simulation of the entrance flow at several flow rates and at various test values of the four parameters.

To improve the efficiency of the estimation software, in this work, only the values of λ_2 and m are optimized simultaneously, which is followed by individual optimization of δ and λ_1. It should be noted that parameters λ_2 and m affect the elongational viscosity only in the power-law region at high

strain rate, whereas δ and λ_1 control the shape of the elongational-thickening portion of the viscosity curve (Fig. 1). In particular, λ_1 determines the strain rate for onset of elongation-thickening region, whereas δ controls the total increase in the viscosity in the thickening region. Since δ and λ_1, and λ_2 and m affect the elongational viscosity in different regions, values of δ and λ_1, and those of λ_2 and m can be optimized independently. Because of this localized effect of δ and λ_1, and that of λ_2 and m, if all the entrance pressure loss data is in the power-law region, optimization of the elongation-thickening parameters is difficult and vice versa.

To optimize the four elongational viscosity parameters, the experimental data for entrance loss is required for at least four different flow rates. Two of these points should be in the power-law region (to determine λ_2 and m). If the polymer melt exhibits the elongation-thickening region, one of the points should be in the elongation-thickening region (to determine δ) and the fourth point should be in the transition region between Newtonian and elongation-thickening behavior (to determine λ_1). Typically, entrance pressure loss vs flow rate data is available at a large number of points ($\gg$4). Since an entrance flow simulation for a fixed set of elongational viscosity parameters and flow rate requires significant amount of computation time (1–10 min on a Sun workstation, depending upon the number of nodes in the finite element mesh and number of iterations required for convergence), and the entrance flow is repeatedly simulated at the entrance loss vs flow rate data points, if all the data points are used in the optimization scheme, a very large computation time is required for estimation of the elongational viscosity parameters. Therefore, a systematic scheme, described in the next paragraph, is employed in this work to select the four entrance loss vs flow rate data points for estimation of the four elongational viscosity parameters.

Estimation procedure for elongational viscosity parameters starts with an initial guess for the four parameters. The software allows the user to specify an initial estimate of the four parameters. Otherwise, the software automatically initializes the elongational viscosity parameters based upon the generalized Newtonian formulation, that is $\eta_e(e_{II}) = 3\eta_s(e_{II})$, or the values obtained by the Binding's analysis.[5] It should be noted that for both of these cases $\delta = 0$, and λ_1 has no affect on elongational viscosity if $\delta = 0$. Therefore, only λ_2 and m are initialized. Since the experimental data at higher flow rate is expected to be in the power-law region, the data point at the highest flow rate and another data point with flow rate of about 1/100 of the highest flow rate are used for estimation of power-law parameters λ_2 and m. Once the two points for estimation of power-law parameters are identified, as shown in Fig. 2, the optimal values of λ_2 and m are determined by alternating the Newton–Raphson method for λ_2 and m. The function f_m and f_{λ_2} are the differences in experimental and predicted values of entrance pressure loss for

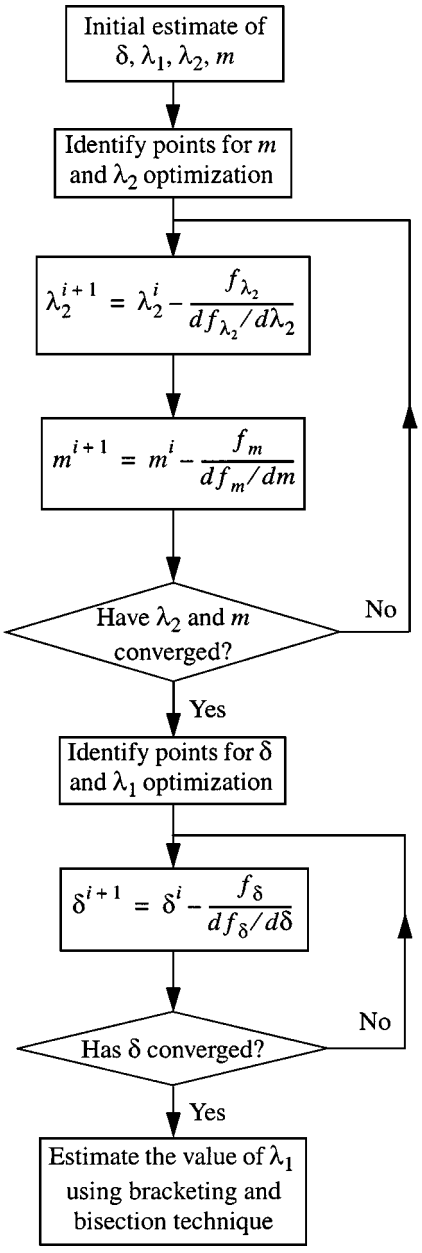

FIGURE 2. Flow chart for optimization of elongational viscosity parameters.

points with the highest flow rate and 1/100 of the highest flow rate, respectively. At this point of the algorithm λ_2 and m have been identified. However, $\delta = 0$ and λ_1 is also unknown. With $\delta = 0$ and using the estimated value of λ_2 and m for the elongational viscosity curve, the data point having the largest difference between experimental and predicted value of entrance loss is used for optimization of δ. If some of the points in the entrance loss vs flow rate data are in the Newtonian range of elongational viscosity, experimental value of entrance loss for these points should match with the predicted entrance loss with $\delta = 0$ in the elongational viscosity model [Eq. (5)]. Therefore, starting with the lowest flow rate, the first data point with experimentally determined entrance loss at least 10% greater than the corresponding prediction is used to optimize the value of λ_1. Before starting the optimization of δ, the parameter λ_1 is initialized to a very large value $\lambda_2 = \lambda_1 \times 10^{10}$, which implies that elongation thickening is assumed to start at a very low elongation rate. Using the point identified above for optimization of δ, as shown in Fig. 2, Newton–Raphson method is used again to estimate the value δ. The function f_δ in Fig. 2 is the difference between experimental and predicted entrance loss for the point being used for optimization of δ. Finally, the parameter λ_1 is estimated by minimizing the entrance loss error for the point identified above for λ_1 optimization. The bracketing and bisection method[11] is used for optimizing the value of λ_1. The Newton–Raphson technique cannot be used for optimizing λ_1, because a change in λ_1 has no effect on entrance flow if the current value of λ_1 is far away from its optimal value. This insensitivity to λ_1 is evident from Fig. 1a, which shows that λ_1 only affects the elongational viscosity curve near the onset of the elongation-thickening region.

It should be noted that during the optimization of the parameter δ, if the value of δ is changed without altering the other elongational viscosity parameters, the elongational viscosity curve in the power-law region is shifted horizontally along the e_{II} axis (Fig. 1b). However, the effect of δ on the power-law region can be countered by changing the value of λ_2. In this work, the value of λ_2 is changed such that the power-law region of the elongational viscosity curve beyond the strain rate for which $\eta_e = \eta_0$ remains unaffected as the value of δ is changed. It can be easily shown that the strain rate for which $\eta_e = \eta_0$ in the power-law region is given by:

$$e^*_{II} = \frac{1}{\lambda_{2p}}\sqrt{(3+\delta_p)^{2/(1-m)} - 1} \qquad (6)$$

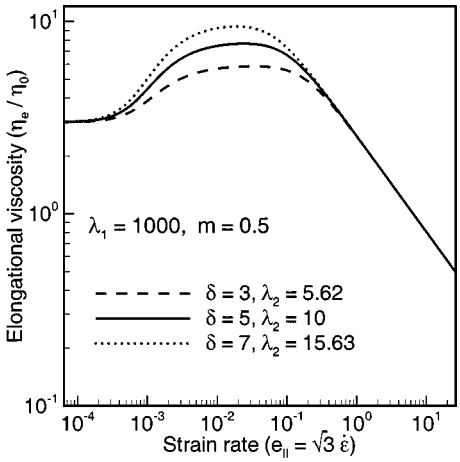

FIGURE 3. Effect of the coordinated change in δ and λ_2 using Eqs. (6) and (7) such that the elongational viscosity in the elongation-thickening region is modified, but the elongational viscosity in the power-law region remains unchanged.

where λ_{2p} and δ_p are the values of λ_2 and δ in the previous iteration. As the value of δ is changed to δ_n in the current iteration, the power-law region of the elongational viscosity curve can be restored to the curve in the previous iteration by changing λ_2 to λ_{2n} given by the following equation:

$$\lambda_{2n} = \frac{1}{e^*_{II}}\sqrt{(3+\delta_n)^{2/(1-m)} - 1} \qquad (7)$$

Figure 3 shows the effect of such a coordinated change in λ_2 and δ given by Eqs. (6) and (7) on the elongational viscosity curve. It is evident from Fig. 3 that only the elongational viscosity curve in the shear thickening region is affected if λ_2 and δ are changed according to Eqs. (6) and (7).

Experimental Data

A Goettfert Rheometer 1000 was used to measure the viscosity and entrance pressure loss. The diameter of capillary in all the dies used was 1 mm. The pressure loss vs capillary length curves for dies with capillary length of 5, 20, 30, and 40 mm were extrapolated to obtain the entrance pressure loss. The Weissenberg–Robinowitch correction was applied to account for the nonparabolic velocity profile. A Bohlin VOR with 25-mm parallel plates was used to measure the shear viscosity at low shear rates. In the experiments, a Low Density Polyethylene (Dow

132i) was used. The entrance pressure loss and shear viscosity was measured for 160 and 175°C.

Results and Discussion

For the results reported in our elongational viscosity estimation papers so far,[10,12] we used the P_2P_1 (quadratic velocity, linear pressure) triangular finite element. Even though the P_2P_1 element accurately predicts the velocity and pressure distributions in an incompressible flow, it requires a relatively large amount of computation time to simulate a flow. To estimate the elongational viscosity, since the entrance flow is simulated repeatedly at various flow rates and for various test values of the elongational viscosity parameters, computational efficiency of the flow simulation is important in order to be able to estimate the elongational viscosity in a reasonable amount of time. To improve the efficiency of the incompressible flow simulation, the $P_1^+P_1$ mini element of Arnold, Brezzi, and Fortin,[13] with the simplified bubble function suggested by Coupez and Marie,[14] has been employed for the results reported in this paper. For a triangular finite element, the simplified bubble consists of three piece-wise linear functions.[14] An advantage of the piece-wise linear bubble is that it allows an exact integration over the triangular finite element. Employing the static condensation technique,[15] the velocity equations corresponding to the bubble node were eliminated at the element level, resulting in the higher computational efficiency of the mini element. To avoid the bubble reconstruction, the nonlinearity in the rheological behavior is treated by projection of the P_1^+ velocity field on the P_1 subspace. To simulate a three-dimensional flow, Coupez and Marie,[14] used the preconditioned conjugate residual (PCR) method for solving the set of simultaneous linear equations. The PCR method was also implemented in this work. However, for a small number of nodes, typically used in a two-dimensional finite element simulation, the direct solution of the linear equations by LU decomposition technique was found to be more efficient than the PCR method. For small number of nodes, better efficiency of the direct solver was also reported by Coupez and Marie.[14] Therefore, a direct solver, using the LU decomposition technique was used for obtaining the results reported here. The finite element mesh used (Fig. 4) has 1633 nodes and 3040 elements.

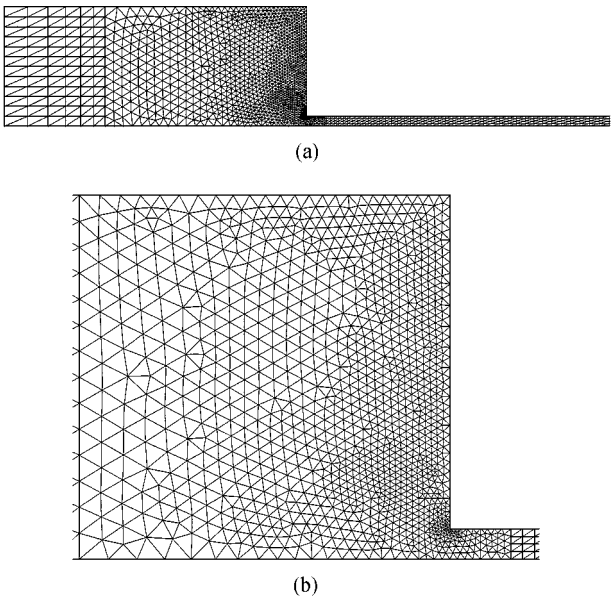

FIGURE 4. Finite element mesh used for the 12:1 entrance flow simulation (a) over the complete flow domain (b) in vicinity of entrant corner.

In this paper, the elongational viscosity for a Dow 132i is estimated at two different temperatures. For Dow 132i at 160 and 175°C, the experimental data for entrance pressure loss at various flow rates is shown in Fig. 5 (F. A. Morrison, personal communication, 2000). As expected, the entrance loss increases significantly as the flow rate is increased. At a fixed flow rate the entrance loss is higher for the lower temperature. The shear viscosity for Dow 132i, which is obtained by fitting the Carreau model to the experimental data, is shown in Fig. 6. The

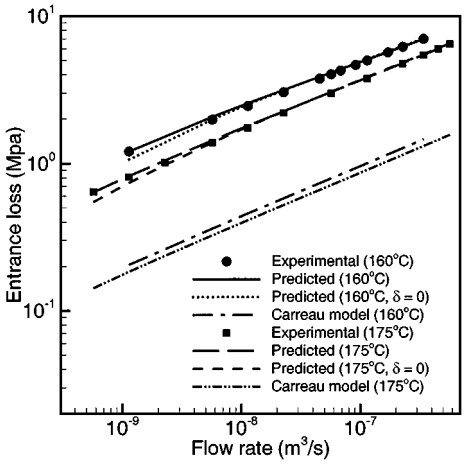

FIGURE 5. Entrance loss vs. flow rate for Dow 132i.

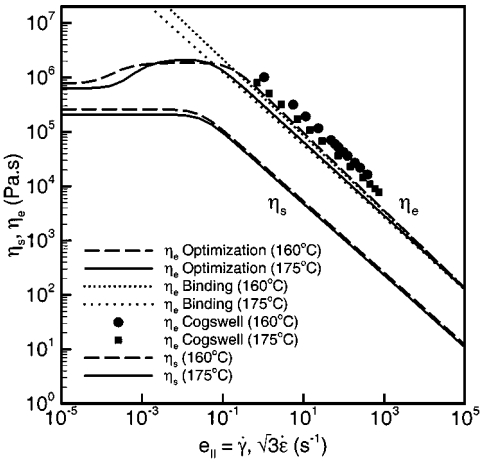

FIGURE 6. Variation of shear (η_S) and elongational (η_e) viscosities of Dow 132i with the second invariant of strain-rate tensor (e_{II}).

Carreau model parameters for the shear viscosity of Dow 132i are as follows (F. A. Morrison, personal communication, 2000):

	η_0 (Pa s)	λ (s^{-1})	n
160°C	2.6×10^5	37.35	0.3409
175°C	2.1×10^5	31.69	0.3409

These Carreau model parameters along with the entrance loss data (shown in Fig. 5) were used in this work to predict the elongational viscosity employing the algorithm discussed earlier in this paper. For the two different temperatures, the predicted elongational viscosity is shown in Fig. 6. It should be noted that the predicted elongational viscosity is plotted against $e_{\text{II}} = \sqrt{3}\dot{\varepsilon}$ (Fig. 6). The power-law parameters for the elongational viscosity were predicted using the entrance pressure loss values for flow rates of 5.65 and 339 mm^3/s for 160°C and for 5.66 and 452 mm^3/s for 175°C. With these control points the predicted elongational viscosity parameters are as follows:

	λ_2 (s^{-1})	m
160°C	1.85	0.28
175°C	2.85	0.32

It is noted that even though in good agreement, these values of λ_2 and m are slightly different from the values reported in Ref. 12. This minor difference in the values of λ_2 and m is expected because the P_2P_1 element was used for the results reported in Ref. 12, whereas the $P_1^+P_1$ element has been employed in this paper. Using these values of the two elongation-thinning parameters, with $\delta = 0$, that is, no elongation thickening, the largest difference in the experimental and predicted entrance pressure loss was obtained at the lowest flow rates in Fig. 5, which are 1.13 and 0.565 mm^3/s for 160 and 175°C, respectively. In our earlier work,[12] the attempt to optimize δ using the entrance loss data at these two points was unsuccessful, because the predicted entrance loss at these two points was found to be insensitive to a change in δ. Since then, the sensitivity of entrance loss to δ was improved in the software, which allowed us to optimize δ and λ_1 in this work. As δ is modified during the optimization process, in order to keep the power-law region of the elongational viscosity curve unaltered, the value of λ_2 was adjusted according to Eqs. (6) and (7). The optimized values of the elongational viscosity parameters for the curves shown in Fig. 6 are as follows:

	δ	λ_1 (s^{-1})	λ_2 (s^{-1})	m
160°C	4.29	6549.7	6.5	0.28
175°C	7.58	1869.1	18.7	0.32

It is evident from Fig. 5, that with $\delta = 0$, i.e. no elongation thickening, the predicted entrance losses at only a few points near the lowest flow rates (one point for 160°C and three points for 175°C) are significantly different that the corresponding predictions with nonzero δ values. Since only a limited experimental data on entrance flow is available in the elongation-thickening region, the elongation thickening regions for 160 and 175°C shown in Fig. 6 may not be very accurate. This low accuracy of the predicted elongation-thickening region is probably causing the two elongational viscosity curves to intersect unexpectedly in the elongation-thickening region. The entrance pressure loss predicted by a generalized Newtonian formulation using Carreau model, which is also shown in Fig. 5, is only about 20% of the corresponding experimental data.

For Dow 132i, the elongational viscosities at 160 and 175°C, predicted by Cogswell's and Binding's analyses are also shown in Fig. 6. Interestingly, even though Cogswell's and Binding's predictions are based upon numerous simplifying assumptions, the elongational viscosity predicted by the two analyses are in good agreement with the predictions from the present work.

For three different flow rates in the range of the experimental data in Fig. 5, unit vectors along the direction of velocity near the abrupt contraction are shown in Fig. 7. In contrast to the results reported in Ref. 6, the recirculation region near the abrupt contraction shrinks as the flow rate is increased. For the velocity distributions at various flow rates reported in Ref. 6, the elongational power-law index (m) was larger than the power-law index (n) for the shear viscosity. With $m > n$, the Trouton ration ($T_r = \eta_e/\eta_s$) increases with flow rate. Accordingly, the recirculating vortex also grows with flow rate. In this work, for Dow 132i, since m is less than n, Trouton ratio decreases as the flow rate is increased. Because of this decrease in Trouton ratio, for Dow 132i, the predicted recirculating vortex shrinks as the flow rate is increased. The velocity distributions shown in Fig. 7 are for 160°C. Similar reduction in recirculation with increasing flow rate was found for 175°C. Also, the recirculation region and the pressure distribution along the channel, predicted by the two different types of finite elements, P_2P_1 and $P_1^+P_1$, were found to be in good agreement.

In closing, it is emphasized that the results reported here should be treated as estimates of the resistance of Dow 132i to an elongational deformation. Even though these could be used as the estimated elongational viscosity of the polymer, because

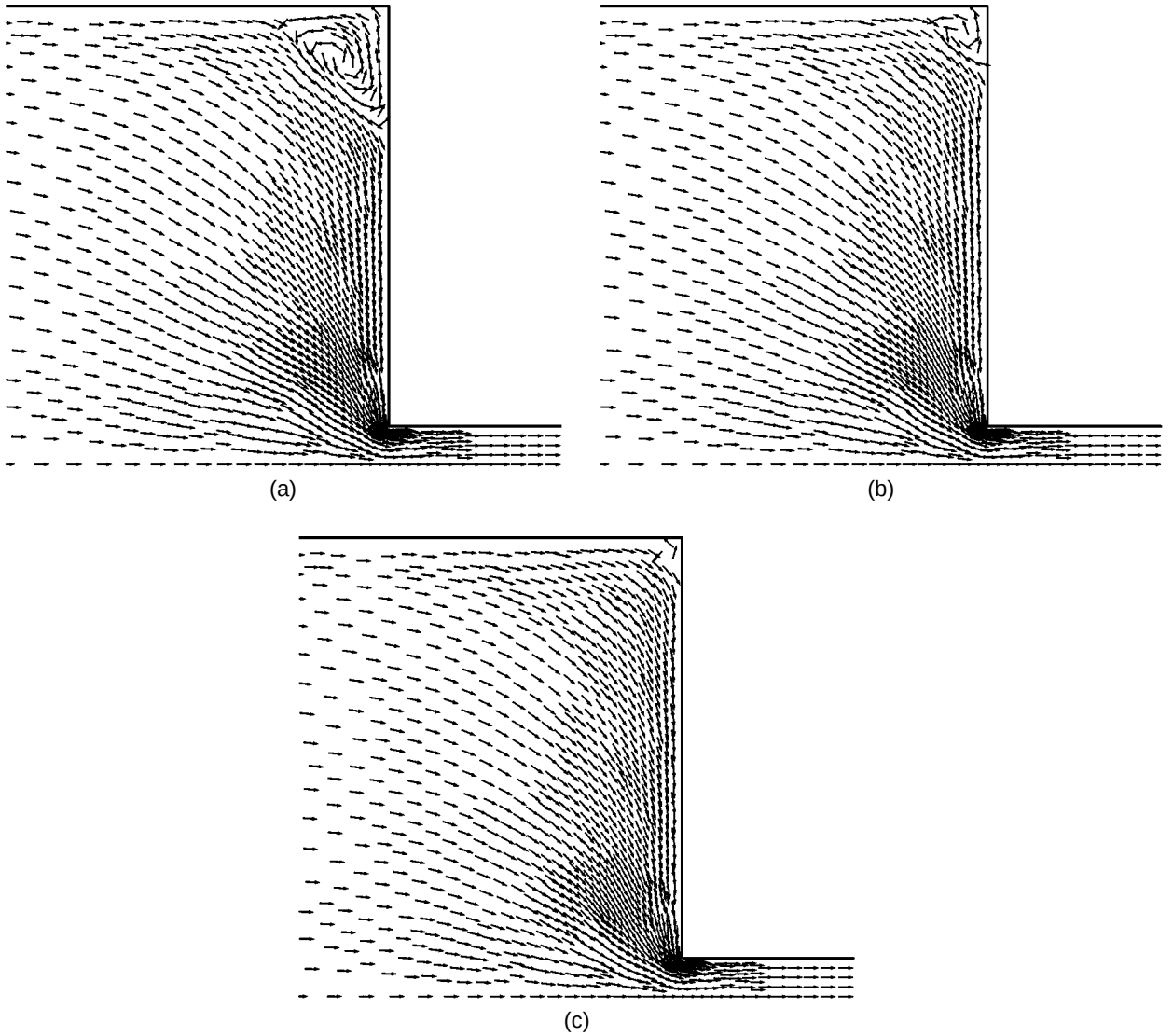

FIGURE 7. Recirculation in an axisymmetric 12:1 entrance flow of Dow 132i at 160°C. The flow rates are 1 mm^3/s (a), 10 mm^3/s (b), and 100 mm^3/s (c).

of the several simplifications in the present analysis, the intrinsic elongational viscosity of the polymer obtained by a direct elongation experiment, can be somewhat different than these estimates. For instance, the first and second normal stress differences, which can also affect the entrance pressure loss, have not been accounted in the present analysis. Even though viscous dissipations can change the temperature of the polymer melt in a capillary rheometer, the simulations reported here are isothermal. The entrance flow is sometimes susceptible to nonaxisymmetric instabilities, which can only be captured in a three-dimensional flow simulation. Also, the present analysis employs a steady state simulation. Therefore, transient flow instabilities, which are sometimes encountered in entrance flow, could not be simulated in the present work. In spite of these simplifications, because of the numerous difficulties associated with the direct measurement of elongational viscosity, the method employed here provides an attractive alternative for estimation of the elongational viscosity of a polymer.

Conclusions

A scheme employing individual parameter optimization has been used to optimize the values of the four parameters in the elongational viscosity model proposed by Sarkar and Gupta.[9,10] By minimizing the difference between the predicted entrance loss and the corresponding experimental values at strategically selected flow rates, the optimization scheme starts by estimating the values of elongation-thinning parameters, which is followed by estimation of the two elongation-thickening parameters. The estimated elongational viscosities for Dow 132i at two different temperatures are reported. The corresponding predictions of elongational viscosity from Binding's and Cogswell's analyses are found to be in good agreement with the present estimations.

Acknowledgment

The author thanks Prof. F. A. Morrison for making the experimental data for entrance pressure loss and shear viscosity available.

References

1. Bird, R. B.; Armstrong, R. C.; Hassager, O. Dynamics of Polymeric Liquids; Wiley: New York, 1987; Vols. 1 and 2.
2. Macosko, C. W. Rheology Principles, Measurements and Applications; VCH: New York, 1994.
3. Meissner, J. Rheol Acta 1969, 8, 78.
4. Cogswell, F. N. Polym Eng Sci 1972, 12, 64.
5. Binding, D. M. J Non-Newtonian Fluid Mech 1988, 27, 193.
6. Gupta, M. Polym Eng Sci 2000, 40, 23.
7. Gupta, M. J Reinforced Plast Composites 2001, 20, 341.
8. Gupta, M. SPE ANTEC Tech Papers 1999, 45, 83.
9. Sarkar, D.; Gupta, M. J Reinforced Plast Composites 2001, 20, 1473.
10. Sarkar, D.; Gupta, M. In CAE and Related Innovations for Polymer Processing; Turng, L. S.; Wang, H. P.; Ramani, K.; Bernard, A. (Eds.); ASME: New York, 2000; MD-Vol. 90, p. 309.
11. Press, W. H.; Flanery, B. P.; Teukolsky, S. A.; Vetterling, W. T. Numerical Recipes; Cambridge University Press: Cambridge, 1989.
12. Gupta, M. SPE ANTEC Tech Papers 2001, 47, 794.
13. Arnold, D. N.; Brezzi, F.; Fortin, M. Calcolo 1984, 21, 337.
14. Coupez, T.; Marie, S. Int J Supercomputer Appl High Performance Computing 1997, 11, 277.
15. Bathe, K. J. Finite Element Procedures; Prentice Hall: Englewood Cliffs, NJ, 1996.